A Preliminary Study of Strong Motion Records in the Sapporo Metropolitan Area during the 2010 Central Ishikari Earthquake

M. Shigefuji, T. Sasatani & N. Takai
Hokkaido University, Japan

SUMMARY:
The Sapporo metropolitan area is located on a deep sedimentary basin in the Ishikari depression, the western part of Hokkaido, Japan. A moderate-size shallow earthquake (Mw 4.6) occurred on December 2, 2010 beneath the southern part of Sapporo city. The record sections of velocity waveforms along a profile in the N30W direction from the epicenter show conspicuous later phases after P- and S-waves. We investigated the observed record sections to understand effects of sedimentary layers on ground motion. The synthetic waveforms by 1-D simulation using the velocity structure model after AIST and the re-determined source parameters reproduce the observed waves. We revealed that the direct and later phases are *diffracted waves* generated when the source is located near the sediment-seismic basement interface. These suggest that the source parameters re-determined in this study and the AIST velocity structure along this profile are reasonable.

Keywords: The Ishikari plain, 3-D velocity structure, The 2010 Central Ishikari earthquake, Diffracted waves

1. INTRODUCTION

The Sapporo metropolitan area is located on a deep sedimentary basin in the Ishikari depression, the western part of Hokkaido, Japan. The population of Sapporo-city is about 2 million, and the high-rise buildings with a height of over 100 m have increased recently. Sapporo-city government carried out the seismic refraction and reflection surveys and the microtremor surveys (Sapporo-city, 2002, 2003, 2004, 2005), in order to construct the 3-D velocity structure model of the Sapporo basin. Recently the National Institute of Advanced Industrial Science and Technology (AIST) developed the 3-D velocity structure model of the Ishikari and Yūfutsu sedimentary basins integrating existing these data (Yoshida *et al.*, 2007).

On December 2, 2010 at 6:44 (JST), a moderate-size shallow earthquake occurred beneath the southern part of Sapporo city in the central Ishikari region; here, we call this event the 2010 Central Ishikari earthquake. The magnitude of this event, according to Japan Metrological Agency (JMA), is *Mj*=4.6. This event is the largest one since the observation had started in this area. This event caused slight damage such as breakage of structures and slide of sloping ground surface around the epicenter. Sapporo district meteorological observatory (2010) reported that strong shaking occurred around the epicenter; seismic intensity (JMA scale) at that area is 4 to 5 lower.

We obtained a lot of strong motion data from the 2010 Central Ishikari earthquake. These data provides a good opportunity for studying effects of sedimentary layers on ground motion. In this paper, first, we re-determine the source parameters using the near-field records by modeling the observed waveforms. Next, we investigate the observed record sections along a profile in the N30W direction to understand a generation mechanism of the conspicuous later phases at the far-field stations.

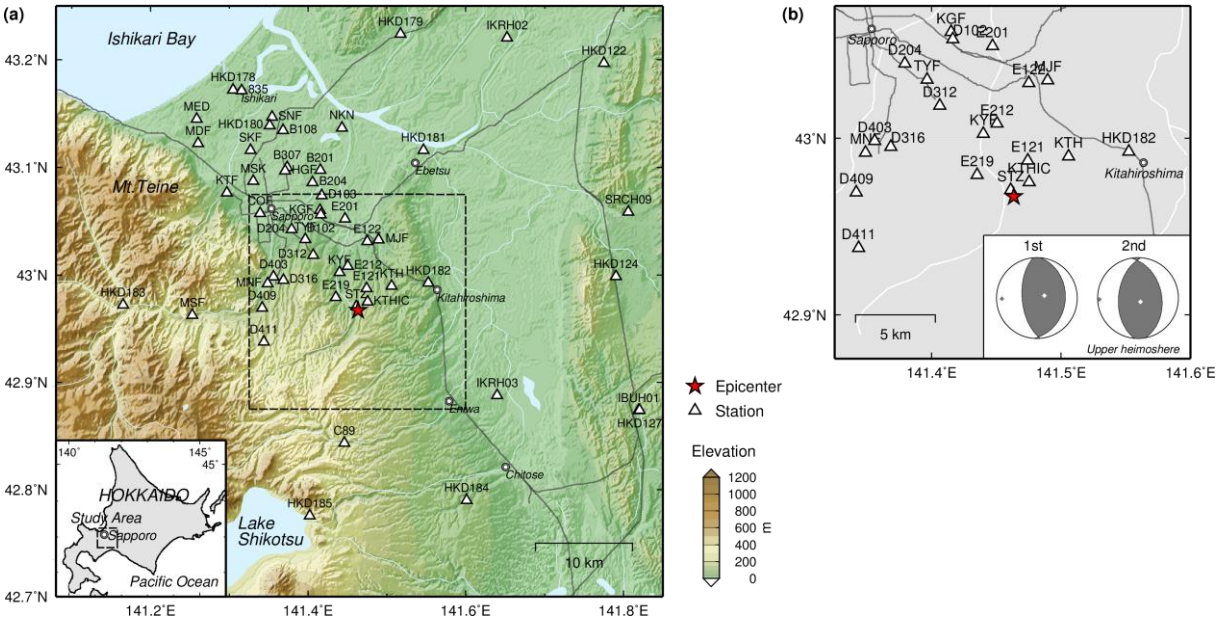

Figure 1. (a) Map of the study area showing epicenter (star) for the 2010 Central Ishikari earthquake, locations of stations used in this study, and outline of area shown in Figure 1b. (b) Map of the area within an epicentral distance of 10 km. The focal mechanisms for the multiple-shock determined in this study are shown. Upper-hemisphere projection is used here.

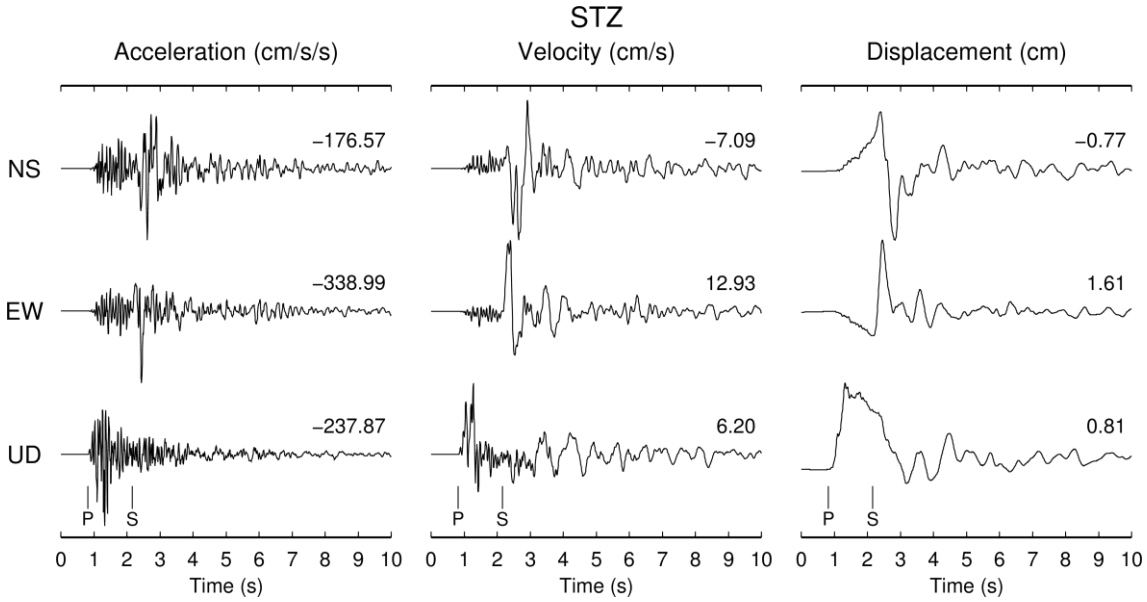

Figure 2. Observed records at the nearest station STZ. Left: acceleration, Middle: velocity, and Right: displacement waveforms. Amplitudes are normalized; numbers attached to each trace show the maximum amplitudes.

Table 1. Source parameters determined in this study.

Origin time (JST)	2010/12/02 06:44:02	
Latitude, Longitude	42.967°N, 141.463°E	
Focal depth [km]	5.0	
Total seismic moment [N-m]	8.41E+15	
	1st event	2nd event
Focal mechanism: strike, dip, rake angle	355, 60, 85	5, 50, 100
Rise time [sec]	0.3	0.4 (delay: 0.17 sec)
Seismic moment [N-m]	3.00E+15	5.41E+15

2. DATA

In the Sapporo metropolitan area we have dense strong motion observation stations (Figure 1a). These stations recorded ground motion during the 2010 Central Ishikari earthquake. We use strong motion records from K-NET, KiK-net of NIED (National Research Institute for Earth Science and Disaster Prevention), the seismic intensity network of Sapporo-city, Hokkaido Gas Corporation, Ueyama Corporation, and Hokkaido University.

Figure 2 shows observed acceleration, velocity, and displacement waveforms at the nearest station STZ located at a distance of about 0.5 km. The velocity and displacement waveforms are obtained by integration of the acceleration waveforms in the frequency domain. In this process we apply a high-pass filter with a cut-off frequency of 0.1Hz (Saito, 1978). The PGA and PGV values are about 340 cm/s/s and 13 cm/s on the EW components. The velocity S- and P- waveforms on the NS and UD components show two pulses. This fact indicates a multiple-shock. The displacement waveforms are strange compared with the acceleration and velocity waveforms. The NS and EW components show long-period motion between P- and S-wave arrivals. These peculiar waveforms may be attributed to the near-, intermediate- and far-field terms (Aki and Richards, 1980); the displacement field due to a point shear dislocation source is given by the sum of these three terms. A few studies analyzed these peculiar waveforms and retrieved important source information (ex., Kosuga, 1996). In the next section, we analyze near-field records from this event to re-estimate the source parameters.

3. RE-ESTIMATION OF SOURCE PARAMETERS

We re-determine the source parameters (epicenter, focal depth, focal mechanism, seismic moment, and moment rate function) of the 2010 Central Ishikari earthquake by modeling the near-field record from stations located within a distance of about 10 km, which are 21 stations as shown in Figure 1b. These observed displacement waveforms show clear near-field term motions.

The source parameters are determined using a grid search. Synthetic waveforms at the near-field stations are considerably sensitive to the focal mechanism. First, we determine the source parameters by modeling velocity and displacement waveforms of 4 stations (STZ, KTHIC, E219, E121) located within a distance of about 3 km, then displacement waveforms of 21 stations located within a distance of about 10 km. The synthetic waveforms are calculated by using the discrete wavenumber (DWN) method (Bouchon, 1981; Takeo, 1985). The 1-D velocity structure used in calculation for each station is assumed based on the AIST 3-D velocity structure model. The optimum epicenter, focal depth and focal mechanism are shown in Figure 1b. The source parameters obtained in this study are summarized in Table 1. The multiple-shock is suggested by the observed records (see Figure 2), so that we estimate two isolated source parameters. Figure 3 shows a comparison of the observed velocity and displacement waveforms at STZ with synthetic ones for the optimum solution. An agreement between the observed and synthetic waveforms is fairly good.

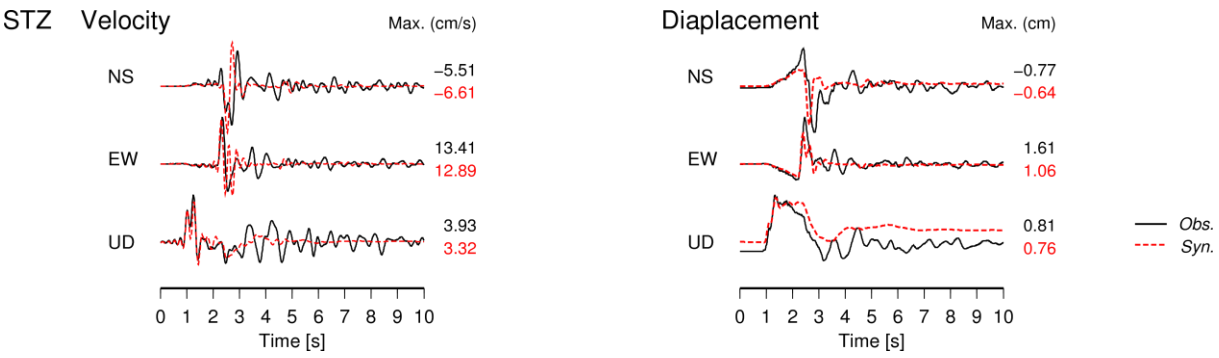

Figure 3. Comparison of the observed velocity and displacement waveforms with the synthetic ones at STZ. The synthetic waveforms are calculated for the source parameters of Table 1.

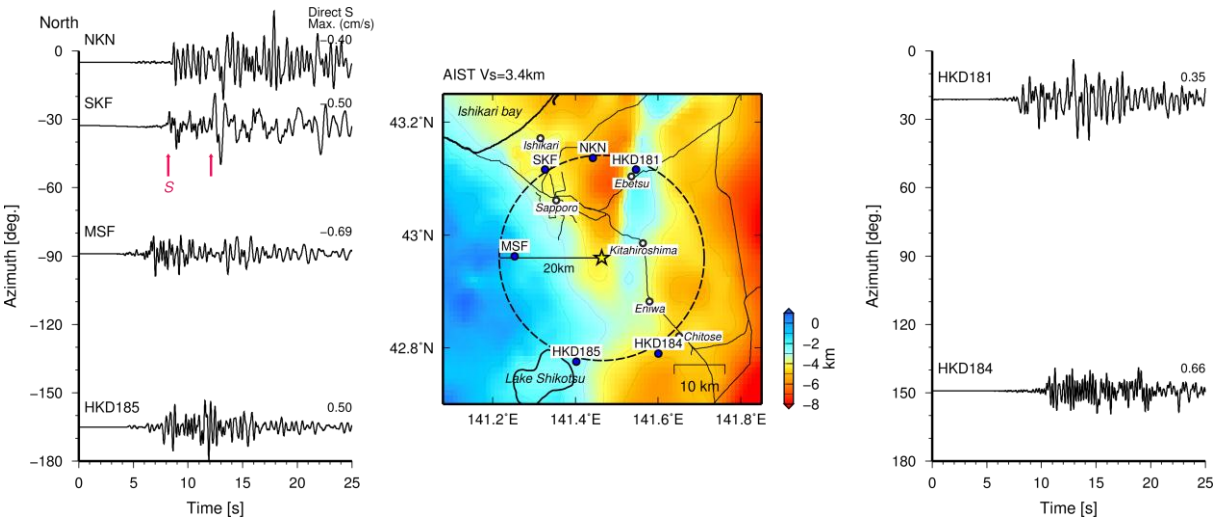

Figure 4. Survey of general features of observed waveforms by comparisons of the traverse component velocity waveforms of stations located at a distance of about 20 km. Amplitudes of each waveform are normalized by the maximum value of the direct S-wave.

4. ANALYSIS OF RECORD SECTIONS ALONG THE PROFILE IN THE N30W DIRECTION

4.1 Finding Conspicuous Later Phases

We analyze the far-filed records to understand effects of sedimentary layers on ground motion. In Figure 4 the middle map shows the depth to the top of the seismic basement in the study area; this figure is constructed from the 3-D velocity structure model by AIST. The undulations are large and the maximum depth is about 7 km at north of the epicenter. This figure shows also a comparison of transverse component velocity waveforms of stations with a distance of about 20 km. Each record shows individual waveforms reflecting site response. We focus on the record of station SKF in the N30W direction, which shows the amplitude of the later phase is larger than that of the direct S-wave. This conspicuous later phase is not clearly visible at other directions.

In order to confirm whether the later phase is visible at other records, we select a profile A-A' in the N30W direction that extends through the station SKF as shown Figure 5a; that length is about 30 km, a total of 16 stations are located fortunately. A record section of the observed velocity waveforms along the profile A-A' are shown in Figure 6. The NS and EW components are rotated into the radial and transverse components using the hypocenter position determined in this study (Table 1). The velocity waveforms are bandpass filtered between 0.1 and 4.0 Hz. The direct S-wave is easily identified on the transverse component as shown by S0 line. The S0 line indicates an apparent velocity of about 3 km/s; this value is nearly the same as S-wave velocity in the seismic basement (Table 2). We can identify the conspicuous later phases at about 4 sec after the direct S-wave; these phases appear at distances greater than about 16 km (HGF) and the travel time is indicated by S1 that is parallel to S0. These record sections show that the later phases produce mostly the peak velocities at distances greater than about 20 km. These features are seen at the S-wave on radial component and the P-wave on vertical component also, although being not so remarkable. An apparent velocity of the direct P-wave on the vertical components (P0) is about 6 km/s; this value is nearly the same as P-wave velocity in the seismic basement. We can identify the conspicuous later phases (P1) at about 2 sec after the direct P-wave; these phases appear at distances greater than about 19 km (SKF), and P1 is parallel to P0.

The above features suggest that these waves propagate horizontal path along the top of the seismic basement; these are similar to the typical features of a *head wave*. It is interested to understand the generation mechanism of the direct and later phases mentioned above. In the next section, we investigate these waves in detail.

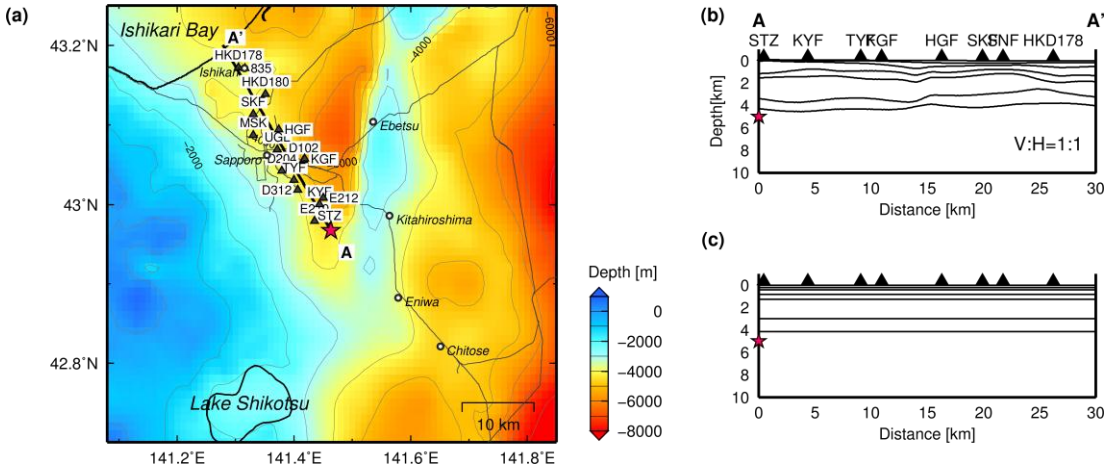

Figure 5. (a) Location map of the profile A-A' in the N30W direction and stations selected for a waveform examination. Depth to the top of the seismic basement after AIST (Yoshida *et al.*, 2007) is also shown. (b) Vertical cross-section of the velocity structure along the profile A-A'. (c) Flat layer velocity structures assumed for a DWN simulation. Material parameters of the velocity structure are shown in Table 2.

Table 2. Material parameters of the velocity structure used in a DWN simulation.

Layer	P-wave velocity *Vp* [km/s]	S-wave velocity *Vs* [km/s]	Density [g/cm^3]	Top of layer [km]	Quality factor *Qp*·*Qs*
1	1.760	0.400	1.980	0.000	50
2	2.090	0.722	1.980	0.227	80
3	2.620	1.196	2.060	0.404	100
4	3.210	1.725	2.270	0.742	150
5	4.070	2.350	2.410	1.166	200
6	5.420	3.131	2.570	2.902	300
7	5.780	3.400	2.770	4.110	340

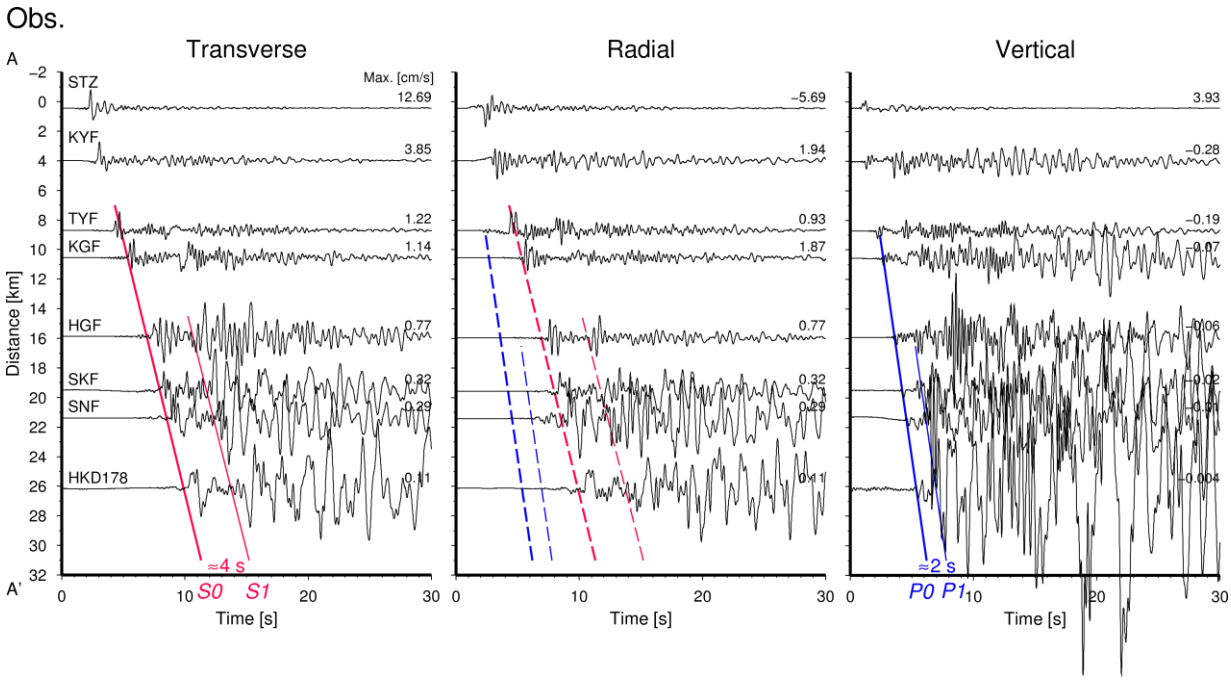

Figure 6. Observed record sections of velocity waveforms along the profile A-A'. Left: Transverse, Middle: Radial, and Right: Vertical components. S0 and S1 lines are the travel-time lines for the direct S and later phases; P0 and P1 lines are the travel-time lines for the direct P and the later phases. Solid lines are obtained based on the observed phases, and dotted lines are referred from the lines on the other components. Amplitudes of each record section are normalized by the maximum value of the direct P- or S-waves.

4.2. Theoretical Consideration of the Wave Field from a Point Source in the Layered Half-Space

Ben-Menahem and Singh (1981) obtained approximate solutions for the wave field from a point source in a layered half-space; these solutions were derived from manipulation of integral paths in the complex wavenumber plane. The solution for a point source in the layer is well known as generation of *diffracted waves* called head waves (or conical waves). They showed the solution for a point source in the half-space also generates *diffracted waves* when the source is located near the interface. The latter case is similar to our observations, because the source is laid beneath the seismic basement. Here we make theoretical consideration of the wave field from a point source in the half-space.

A simple layered half-space is assumed as shown in Figure 9. The S-wave velocity of the layer is 1.4 km/s and that of the half-space is 3.4 km/s, and the thickness of the layer is 4 km. The point source is the pure strike slip fault with the northward strike. The moment rate function has the bell shape with the pulse width of 0.5 sec. The observation array is located in the direction of N90E. In this case, only SH-waves radiate from the source in the direction of N90E. We calculate exactly the synthetic waveforms by using the DWN method.

Figure 7a shows the record section in case of the focal depth of 5 km. The direct waves have an apparent velocity of 3.4 km/s, which is the S-wave velocity of the half-space. This suggests these waves are *diffracted waves*. A few later phases appear after the direct wave and they have the same apparent velocity as the direct waves. The time interval between the direct wave and the first later phase and that between the first later phase and the second one are same. Figure 7b is the same as Fig. 7a, but the focal depth of 10 km. The direct waves in Figure 7b have the same apparent velocity of 3.4 km/s. However, appearance of later phases is strongly different from Figure 7a; the apparent velocity is the same as the direct wave, but the amplitudes are significantly small compared with Figure 7a. The solution by Ben-Menahem and Singh (1981) showed these features qualitatively.

Next we examine the absolute amplitudes for the direct waves and the first later phases. Figure 8 shows the attenuation relations for the direct waves and the first later phases. The direct waves in case of the 5 km depth attenuate with R^{-2} at distances greater than 10 km, where R is the epicentral distance; this nature is the same as the attenuation relation of the head waves. An interesting point is that the amplitudes of the direct waves in case of the 10 km depth are larger than those in case of the 5 km depth at distances greater than 10 km, despite the smaller distance in case of the 5 km depth. On the other hand, the amplitudes of the first later phases in case of the 5 km depth are greater than those in case of the 10 km depth. Furthermore, in case of the 5 km depth, the amplitudes of the later phases are larger than those of the direct waves at distances greater than 20 km; the amplitudes of the later phases are smaller than those of the direct waves in case of the 10 km depth. These features are useful to determine the focal depth based on examination of the observed direct waves and later phases.

It may be somewhat difficult for the record sections shown in Figure 7 to understand the generation process of the *diffracted waves*. So we make the finite difference method (FDM) simulation (Aoi and Fujiwara, 1999; Pitarka, 1999) under the same conditions used in the DWN simulation. Figure 9 shows snapshots of the wave field on the vertical section from a point source in the half-space; the focal depth is set at a depth of 5 km. We can understand above mentioned features by interpreting wavefront systems shown there. For instance, the interval time between the direct wave and the first later phase shown in Figure 7a is directly related the travel time difference due to a multiple reflection at the free surface and the interface; the incident angle is fixed to be the critical angle. Furthermore, the later phases in Figure 7a result from the multiply reflected waves between the free surface and the interface.

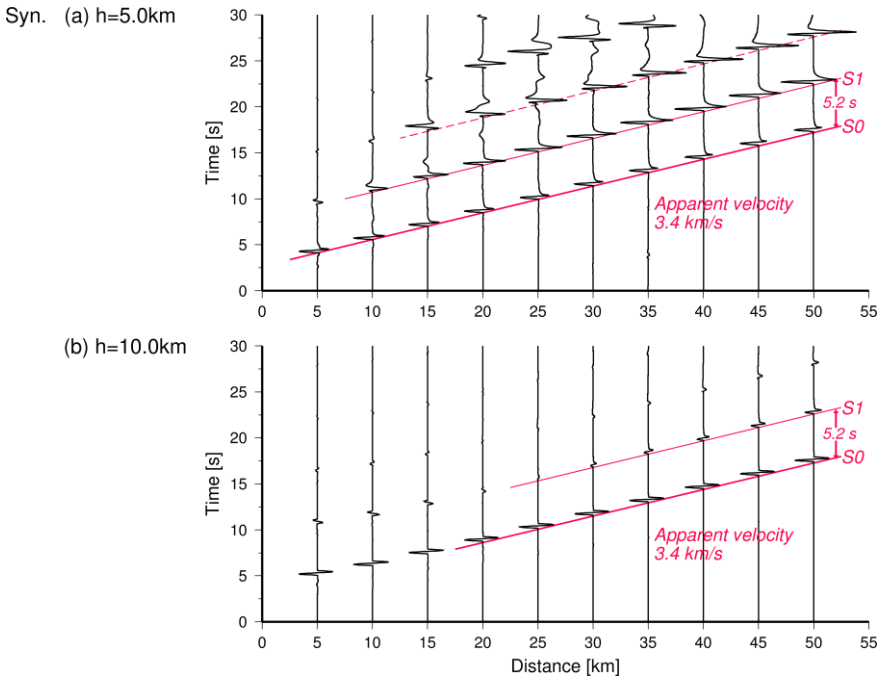

Figure 7. Synthetic record sections in case of the focal depth of 5 km (a), 10 km (b). Amplitudes of each record section are normalized by the maximum value of the direct S-wave. For S0 and S1, see captions in Figure 6.

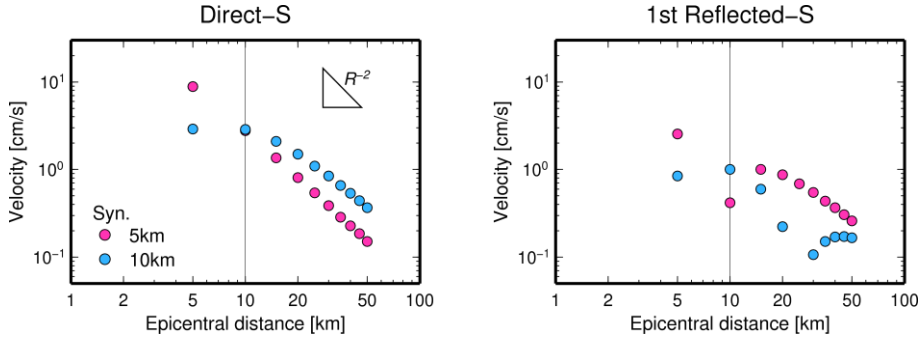

Figure 8. Attenuation relations of the synthetic direct S-wave (left) and first reflected S-wave (right) for the focal depth of 5, 10 km. *R* indicates the epicentral distance. Amplitude is defined as a double-amplitude.

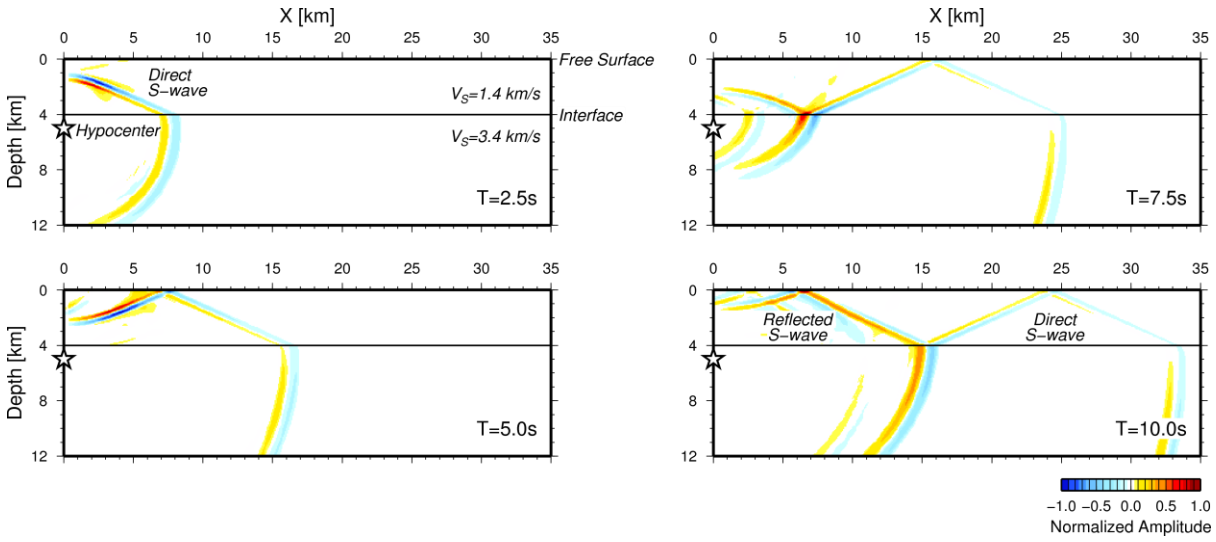

Figure 9. Snapshots of vertical section at times *T*=2.5, 5.0, 7.5, 10.0 sec after origin time for the focal depth of 5 km. Amplitudes of each snapshot is normalized by the maximum value of each time.

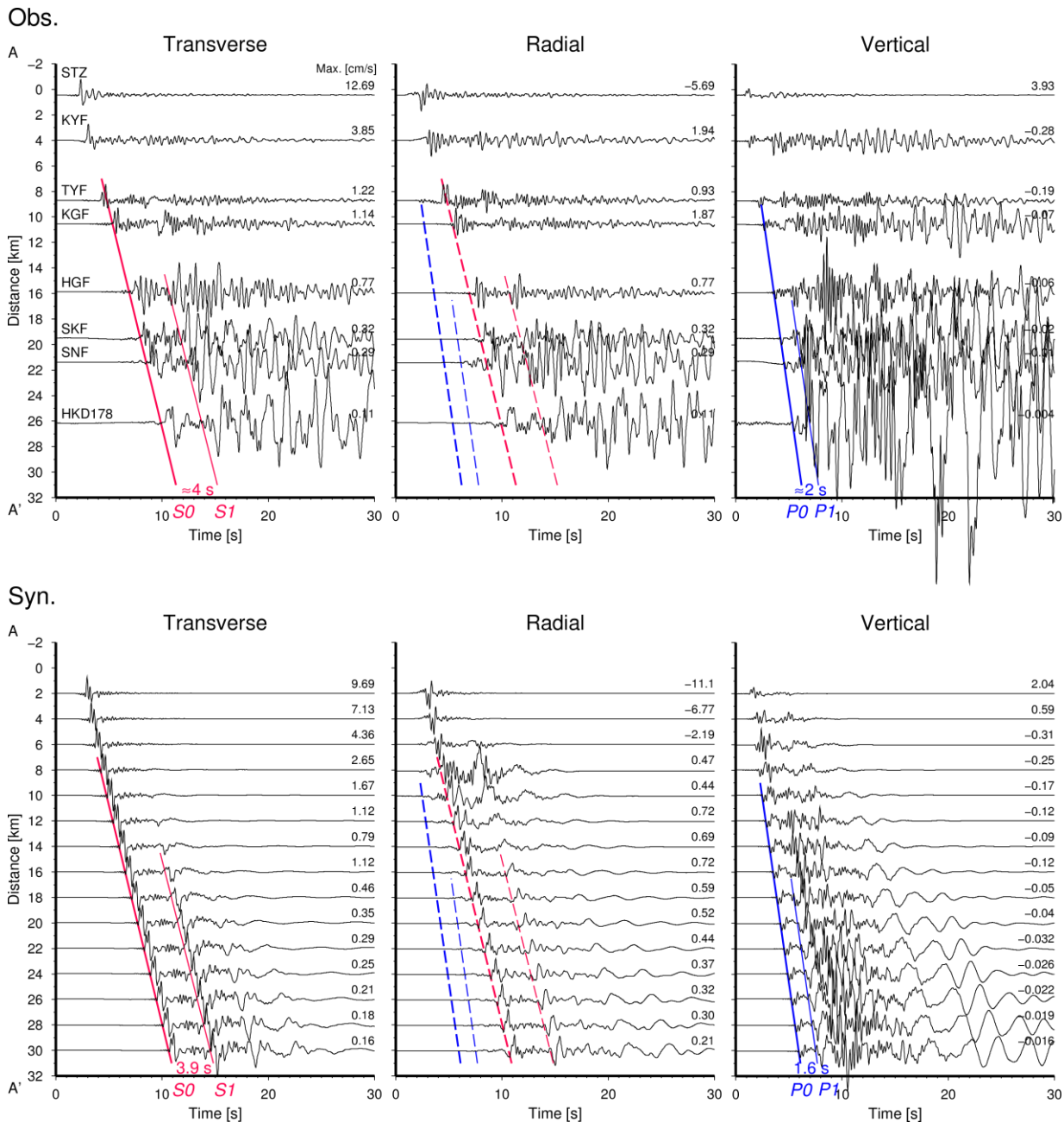

Figure 10. Comparisons of the observed record sections along the profile A-A' (upper) with the synthetic ones (lower). Amplitudes of each record section are normalized by the maximum value at the direct-wave. For P0, P1, S0 and S1, see captions in Figure 6.

4.3 1-D Simulations of Record Sections along the Profile in the N30W Direction

We make a 1-D simulation to understand the generation mechanism of the conspicuous later phases along the profile A-A' from the 2010 Central Ishikari earthquake using DWN method. As shown in the vertical cross-section of the profile A-A' (Figure 5b), the seismic basement is roughly flat and the depth is about 4 km. Undulation in sedimentary layers is not so strong, so that velocity structure used in the DWN simulation is assumed as shown in Figure 4c; material parameters of the velocity structure are listed in Table 2. A station array is located from 2 to 30 km at intervals of 2 km along the profile A-A'. We use the source parameters determined in this study (Table 1).

Figure 10 shows comparisons of the observed record sections along the profile A-A' with the synthetic ones. Velocity waveforms are bandpass filtered between 0.1 and 4.0 Hz. We confirm that the observed

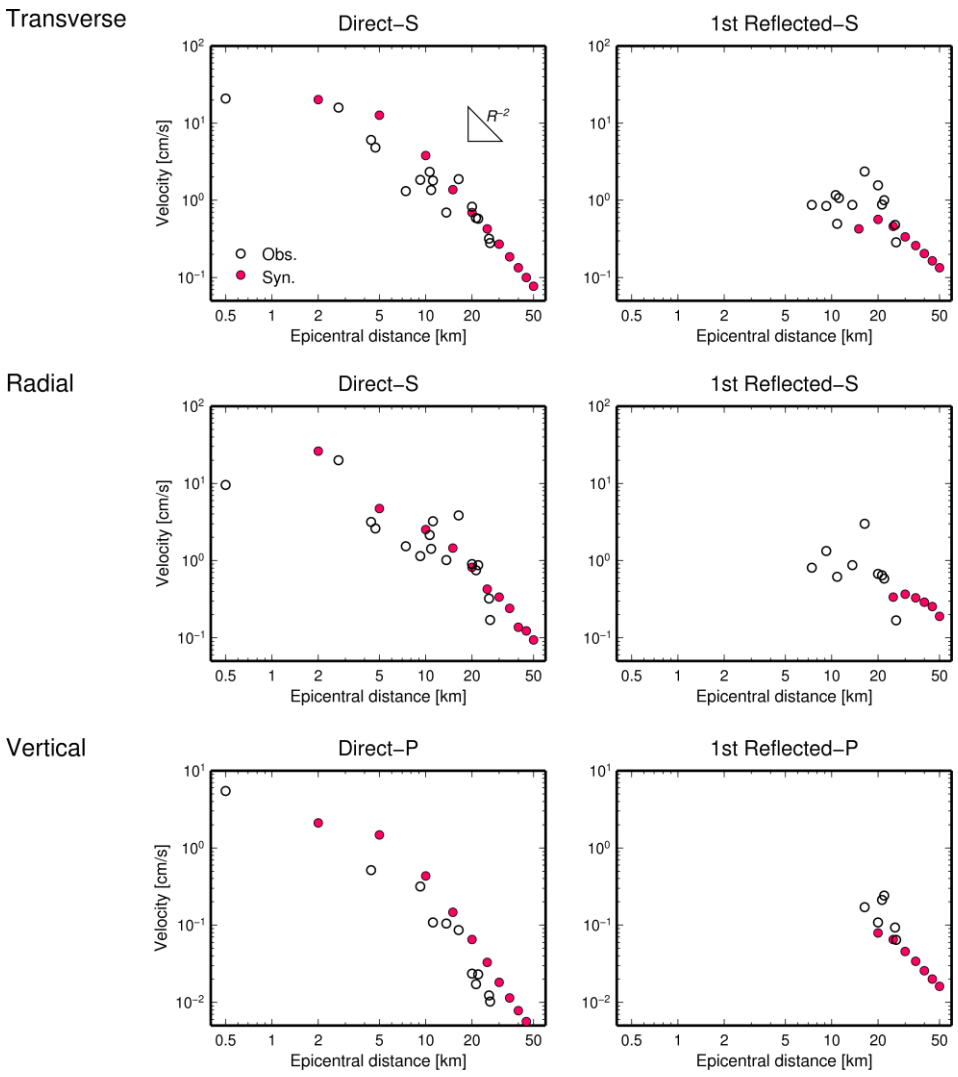

Figure 11. Comparison of the observed attenuation relations with the synthetic ones. Left: direct wave, Right: first reflected wave. *R* indicates the epicentral distance. Amplitude is defined as double-amplitude.

later phases after the direct S- and P-waves are well reproduced by the simulation. On the transverse component of the synthetic record section, the direct S-waves (S0) have an apparent velocity of about 3 km/s, corresponding to the S-wave velocity in the seismic basement (Table 2). The first reflected S-waves (S1) appear at distances greater than about 16 km, which have the same apparent velocity as the direct waves. The travel time difference between S0 and S1 is 3.9 sec, which is nearly the same as the observed value (~ 4 sec). In Figure 11, we compare the observed attenuation relations with the synthetic ones. The synthetic amplitudes of the direct S-wave attenuate with R^{-2} at distances greater than about 8 km and are smaller than those of the first reflected wave at distances greater than about 20 km, which agree with the observed ones well. Similarly, this coincidence is confirmed on radial component. Moreover, on the vertical component of the synthetic record section, the direct P-waves (P0) have an apparent velocity of about 6 km/s, corresponding to the P-wave velocity in the seismic basement (Table 2). The first reflected P-waves (P1) show the feature of the diffracted waves at distances greater than about 18 km (Figure 10). The travel time difference between P0 and P1 is 1.6 sec, which is nearly the same as observed value (~ 2 sec). The synthetic amplitudes of the direct S-wave attenuate with R^{-2} at distances greater than about 10 km and are smaller than those of the first reflected wave at distances greater than about 20 km, which agree with the observed ones relatively well as shown in Figure 11.

On the basis of the above considerations, we find that the conspicuous later phases seen at the profile A-A' are the diffracted waves besides the multiply reflected waves. We conclude that the synthetic

waveforms relatively well reproduce the observed ones, therefore the focal depth of this event is 5 km; a tentative simulation for a depth of 6 km generate no strong later phases. This revealed that the source parameters re-determined in this study and the velocity structure along the profile A-A' are reasonable.

5. CONCLUSIONS

We re-determined the source parameters of the 2010 Central Ishikari earthquake using the near-field records. Next, we investigated the observed record section along the profile in the N30W direction to understand the generation mechanism of the conspicuous later phases at the far-field stations. The synthetic waveforms calculated by using the re-determined source parameters and the AIST velocity structure along the profile well reproduced the observed later phases. We revealed that the direct and later phases are *diffracted waves* generated when the source is located near the sediment-seismic basement interface. The generation of the diffracted wave strongly depends on the focal depth, strictly speaking, on the distance between the source and the top of the seismic basement. The analysis of the diffracted wave is important to verify the structure and source parameters. From these facts, we concluded that the source parameters re-determined in this study and the AIST velocity structure along the profile are reasonable. However, this study is a preliminary one because the target area was limited and 1-D simulation was used. Comparing the observed record sections and synthetic ones (see Figure 10), the later phase caused by 3-D structure does not reproduce. We are planning to make a 3-D simulation to verify the AIST velocity structure of the Sapporo metropolitan area.

ACKNOWLEDGEMENT

We would like to thank NIED, the seismic intensity network of Sapporo city, JMA, Hokkaido Gas Corporation, Ueyama Corporation, and Hokkaido University for providing the strong motion data. We would particularly like to thank Masahiro Ichiyanagi for providing strong motion data. Most figures were drawn by GMT (Generic Mapping Tools, Wessel and Smith, 1991). This research was partially supported by the Ministry of Education, Science, Sports and Culture, Grants-in-Aid for Scientific Research, 21241044.

REFERENCES

Aki, K. and P. G. Richards (1980). Quantitative Seismology, W. H. Freeman and Company, 932.

Aoi, S. and H. Fujiwara (1999). 3-D finite-difference method using discontinuous grids, *Bull. Seismol. Soc. Am.*, **89**, 918-930.

Ben-Menahem, A. and S. J. Singh (1981). Seismic waves and sources, Springer-Verlag GmbH, NY, 1108.

Bouchon, M. (1979). Simple method to calculate Green's functions for elastic layers media, *Bull. Seismol. Soc. Am.*, **71**, 989-971.

Kosuga, M. (1996). Near-field moment tensor inversion and stress field in northeastern Japan, Tohoku university, Ph.D. thesis.

Pitarka, A. (1999). 3D Elastic finite-difference modeling of seismic motion using staggered grids with nonuniform spacing, *Bull. Seismol. Soc. Am.*, **89**, 54-68.

Saito, M. (1978). An automatic design algorithm for band selective recursive digital filters, *Geophys. Exploration*, 240-263 (in Japanese with English abstract).

Sapporo District Meteorological observatory (December 3, 2010). Reports of the earthquake in the central Ishikari region on Decem-ber 2, Press release, http://www.jma-net.go.jp/sapporo/news/2010/sp_press 101203.pdf (in Japanese).

Sapporo-city (2002, 2003, 2004, 2005). Estimation of Subsurface Structures of Ishikari basin, http://www.hp 1039.jishin.go.jp /kozo/eqkozo frm.htm.

Takeo, M. (1985). Near-field synthetic seismograms taking into accunt the effects of an elastic attenuation on seismograms caused by asedimentary layer-, Meterol. *Geophys.*, **36**, 235-257 (in Japanese with English abstract).

Wessel, P. and Smith W. H. F., (1991), Free software helps map and display data, *EOS Trans. AGU*, **72**, 441.

Yoshida, K., M. Yoshimi, H. Suzuki, M. Morino, F. Takizawa, H. Sekiguchi, and H. Horikawa (2007). 3D velocity structure model of the Ishikari and Yūfutsu sedimentary basins, *Annual report on active fault and paleoearthquake researches*, **7**, 1-29 (in Japanese with English abstract).